Facile Synthesis of Highly Efficient One-Dimensional Plasmonic Photocatalysts through Ag@Cu₂O Core−Shell Heteronanowires

Jinyan Xiong,[†] Zhen Li,*,[†,‡] Jun Chen,[§] Shanqing Zhang,[⊥] Lianzhou Wang,[∥] and Shixue Dou[†]

[†]Institute for Superconducting & Electronic Materials and [§]Intelligent Polymer Research Institute, The University of Wollongong, Wollongong NSW 2500, Australia

[⊥]Centre for Clean Environment and Energy Environmental Futures Centre, Griffith School of Environment, Griffith University, Southport QLD 4222, Australia

[∥]Nanomaterials Centre, School of Chemical Engineering & Australian Institute for Bioengineering and Nanotechnology, The University of Queensland, Brisbane QLD 4072, Australia

[‡]School of Radiation Medicine and Radiation Protection, Soochow University, 199 Ren Ai Road, Suzhou Industrial Park, Suzhou 215123, China

S *Supporting Information*

ABSTRACT: A novel class of one-dimensional (1D) plasmonic Ag@Cu₂O core−shell heteronanowires have been synthesized at room temperature for photocatalysis application. The morphology, size, crystal structure and composition of the products were investigated by XRD, SEM, TEM, XPS, and UV−vis instruments. It was found the reaction time and the amount of Ag nanowires play crucial roles in the formation of well-defined 1D Ag@Cu₂O core−shell heteronanowires. The resultant 1D Ag@Cu₂O NWs exhibit much higher photocatalytic activity toward degradation of organic contaminants than Ag@Cu₂O core−shell nanoparticles or pure Cu₂O nanospheres under solar light irradiation. The drastic enhancement in photocatalytic activity could be attributed to the surface plasmon resonance and the electron sink effect of the Ag NW cores, and the unique 1D core−shell nanostructure.

KEYWORDS: *Ag@Cu₂O, one-dimensional structure, core−shell nanowires, plasmonic photocatalysts*
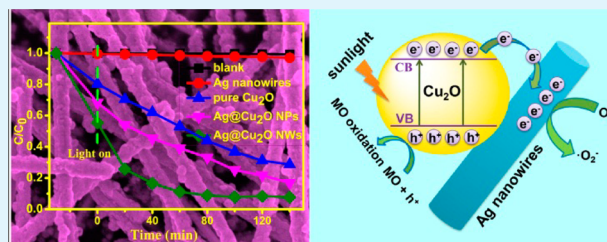
1. INTRODUCTION

The synthesis of one-dimensional (1D) nanostructures and their potential applications in solar energy conversion have attracted much recent interest because of their unique 1D geometry with fast and long-distance electron transfer, superior electron conductivity and mobility, larger specific surface area, light-harvesting efficiency, and length-to-diameter ratio, and high adsorption capacity.[1−16] An important application of 1D nanostructures is in photocatalytic degradation of organic pollutants, and recent decades have witnessed an exponential growth in the design and fabrication of highly efficient and active photocatalysts due to the growing awareness of environmental pollution issues and safety considerations. Various semiconducting nanophotocatalysts, especially metal oxide semiconductors such as TiO₂ and ZnO, are being extensively investigated.[6,7,17−19] The wide band gap of some metal oxides limits their light absorption in the UV region, however, leading to less use of sunlight.[20] To effectively utilize sunlight, noble plasmonic nanostructured metals, such as Au, Ag, and Pt, are deposited on the surface of semiconductors. The metals act as electron traps that introduce efficient interfacial charge separation in the composites, leading to a drastic improvement in photocatalytic activity over an extended wavelength range.[21−24] Metal nanoparticles are most com-

monly used, and they can also be attached to the surface of semiconductors to form core−satellite or core−shell semiconductor@metal nanostructures. The external metal nanoparticles are exposed to reactants and the surrounding medium, however, which could cause corrosion and detachment from the photocatalysts.[25−27] An alternative option is to construct core−shell metal@semiconductor structures.

In addition to the use of plasmonic metal nanostructures, the selection of narrow-band gap semiconductor photocatalysts can also effectively improve absorption of light harvesting. Cuprous oxide (Cu₂O) is one such attractive and environmentally friendly p-type direct semiconductor, with a small band gap (2.17 eV) and unique optical and electrical properties, which make it an appealing candidate for photocatalytic applications.[28−33] To overcome the aforementioned disadvantages of semiconductor-core@metal-shell plasmonic heterostructured photocatalysts, and to further enhance the photocatalytic performance of pure Cu₂O, researchers have widely chosen metal-core@Cu₂O-shell heteronanostructures, such as Cu@Cu₂O core−shell microspheres,[34] Ag@Cu₂O core−shell nano-

particles,[26] and Au@Cu$_2$O core−shell cubes and octahedra,[35] as photocatalysts in recent years. Compared with other noble metals, Ag is more attractive because of its high electrical and thermal conductivity, antibacterial characteristics, low cost, and nontoxicity. Ag nanostructures exhibit a wealth of optical and photoelectrochemical properties directly related to their geometry-dependent surface plasmon resonances, which makes 1D Ag nanostructures great potential candidates in the field of photocatalysis.[25,36−41] However, there is still no report on highly efficient plasmonic heterostructured photocatalysts based on 1D Ag-core@Cu$_2$O-shell architectures to the best of our knowledge, which might be able to fully take advantage of the potential of 1D nanostructures.

Herein, a general procedure for rapid fabricating 1D Ag@Cu$_2$O core−shell heteronanowires for photodegradation of organic dyes is reported. The core−shell heteronanowires are made by overgrowth of Cu$_2$O nanocrystals on the surface of as-prepared Ag nanowires (NWs) via a simple solution process (Scheme 1). The resultant 1D core−shell Ag@Cu$_2$O nanowires show superior photocatalytic degradation of methyl orange (MO) to core−shell Ag@Cu$_2$O nanoparticles and pure Cu$_2$O nanospheres.

Scheme 1. Schematic Illustration of the Plausible Formation Process of the 1D Ag@Cu$_2$O Core−Shell Hetero-Nanowires
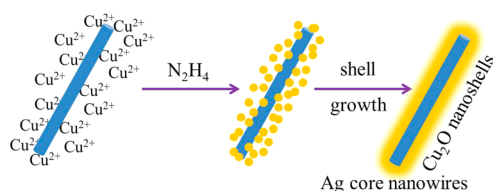
2. EXPERIMENTAL SECTION

Materials. Silver nitrate (AgNO$_3$), hydrazine solution (35 wt % in H$_2$O), sodium chloride (NaCl), and polyvinylpyrrolidone (PVP40) were purchased from Sigma-Aldrich. Copper(II) nitrate 3-hydrate (Cu(NO$_3$)$_2$·3H$_2$O) and MO were purchased from BDH laboratory supplies. Ethylene glycol (EG) was purchased from Alfa Aesar. All of the chemicals were analytical grade and used directly without further purification.

Sample Preparations. Ag nanowires (Ag NWs) were fabricated by a modified polyol process.[42] In a typical synthesis, 10 mL of EG containing PVP40 was loaded into a 25 mL vial, and heated with magnetic stirring in an oil bath at 120 °C for 1 h. One milliliter of NaCl in EG solution (1 mM) was then quickly added, and stirring for another 5 min. Finally, AgNO$_3$ (0.1 M solution in EG) was added to the mixture. The mixture solution was then heated at 120 °C with magnetic stirring for 1 h, yielding the gray Ag NWs.

Ag nanoparticles (Ag NPs) were prepared by the similar procedure without NaCl.

Core−shell Ag@Cu$_2$O heteronanowires were synthesized by a simple solution process used for the synthesis of Au@Cu$_2$O nanoparticles with some modifications.[43] Typically, 8 mL of freshly prepared Ag NW solution was added into 50 mL of 0.05 M Cu(NO$_3$)$_2$·3H$_2$O aqueous solution under constant magnetic stirring for 30 min. Then, 100 μL of N$_2$H$_4$·H$_2$O solution was added into the reaction mixture. The reaction mixture was stirred for 30 min, and then the resultant Ag@Cu$_2$O core−shell nanowires were separated by centrifugation, and washed with deionized water and absolute ethanol to remove impurities, and then dried at 60 °C.

Core−shell Ag@Cu$_2$O heteronanoparticles were prepared using the similar approach to Ag@Cu$_2$O core−shell heteronanowires, except 8 mL of Ag NPs solution was added rather than Ag NWs solution.

Pure Cu$_2$O nanospheres were prepared using the above similar procedure without Ag solution.

Characterization. The X-ray diffraction (XRD) measurements were performed on a GBC MMA X-ray diffractometer using Cu Kα_1 radiation (40kV). The XRD patterns were recorded from 20° to 80° with a scanning rate of 2°/min. SEM images were taken using a field-emission scanning electron microscope (JSM-7500FA, JEOL) operated at an accelerating voltage of 5 kV. TEM images were recorded on a field-emission transmission electron microscope (JEM-2011, JEOL), using an accelerating voltage of 200 kV. UV−vis absorption spectra were taken at room temperature on a UV-3600 (Shimadzu) spectrometer. X-ray photoelectron spectroscopy (XPS) was performed by a VG Scientific ESCALAB 2201XL photoelectron spectrometer with Al Ka X-ray as the excitation source to analyze samples' elemental composition. Analysis of the XPS data was carried out using the commercial CasaXPS 2.3.15 software package.

Photocatalytic Test. Photocatalytic activity of the as-synthesized Ag@Cu$_2$O core−shell nanowires was evaluated by the degradation of MO under the irradiation of a LSC-100 Solar Simulator (Newport). In an experiment, 5 mg of photocatalyst was added into 50 mL of MO solution at room temperature. Prior to irradiation, the suspension was stirred in the dark to ensure the establishment of an adsorption−desorption equilibrium between the photocatalysts and MO. Then the solution was exposed to solar light irradiation under magnetic stirring. At each irradiation time interval, 2 mL of the suspension was collected and then centrifuged to remove the photocatalysts. The concentration of MO was analyzed by a Shimadzu UV-3600 spectrophotometer, and the characteristic absorption of MO at 464 nm was used to evaluate its photocatalytic degradation. All of the measurements were carried out at room temperature.

3. RESULTS AND DISCUSSION

Figure 1A−C shows typical scanning electron microscope (SEM) images of the Ag nanowires prepared by a modified polyol reduction process,[42] which serve as templates for the subsequent heterogrowth of Cu$_2$O nanoshells to form Ag@Cu$_2$O core−shell nanowires. These Ag nanowires are well crystallized (see Figure S1 in the Supporting Information) and possess relatively smooth surfaces, and have an average diameter of about 100 nm and a length of about 10 μm. SEM images of the Ag@Cu$_2$O core−shell heteronanowires are displayed in Figure 1D−F, which clearly show that the surface of the Ag@Cu$_2$O core−shell heteronanowires is not as smooth as that of the Ag NWs, due to the coating by a layer of dense Cu$_2$O nanoparticles. The enlarged SEM image (Figure 1F) reveals that many tiny Cu$_2$O nanoparticles have densely grown on the entire surface of the Ag nanowires, including both ends, to form a rough surface.

Transmission electron microscopy (TEM) was used to further characterize Ag@Cu$_2$O core−shell heteronanowires (Figure 1G, H and Figure S2 in the Supporting Information). Figure 1G clearly shows individual Ag@Cu$_2$O heteronanowire with a rough surface and a diameter of 170 nm, which consists of 90 nm Ag core and 40 nm Cu$_2$O shell. The interface between Ag nanowire and Cu$_2$O nanoparticles is also clearly observed. The HRTEM image in Figure 1(H) shows the lattice fringes of 0.25 and 0.24 nm, which correspond to Cu$_2$O (111) and Ag (111), respectively. The similar lattice fringes are attributed to the same cubic crystal structures of Ag and Cu$_2$O and their small lattice mismatch (i.e., $a_{Ag} = 4.08$ Å and $a_{Cu2O} = 4.27$ Å). The distribution of elements in the Ag@Cu$_2$O core−shell heteronanowires is shown in Figure 1I. The upper-left image in Figure 1I is the area where the elemental mapping was performed. The green, blue, and red colors represent the distribution of the elements silver, copper, and oxygen, respectively. The presence of the three elements in the
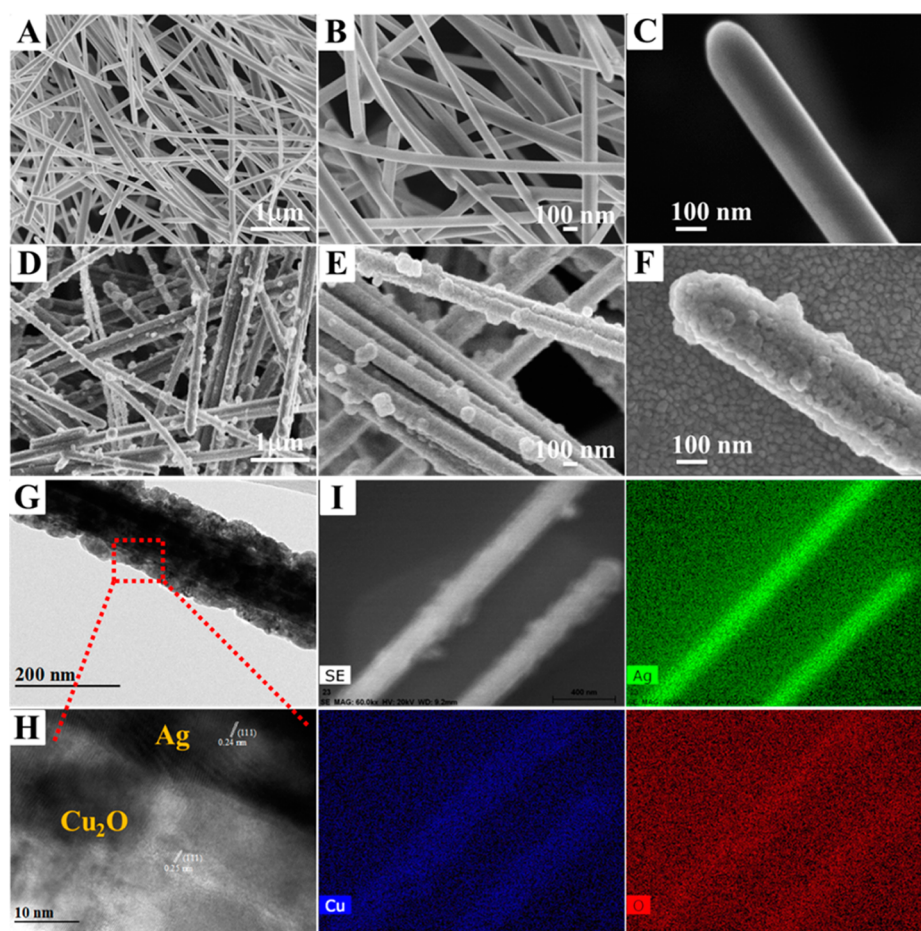
Figure 1. (A−C) SEM images of the Ag NWs, (D−F) SEM images of the as-prepared Ag@Cu$_2$O core−shell heteronanowires. (G) TEM image and (H) HRTEM of an individual Ag@Cu$_2$O core−shell heteronanowire. (I) EDX elemental mapping analysis of the Ag@Cu$_2$O core−shell heteronanowires.
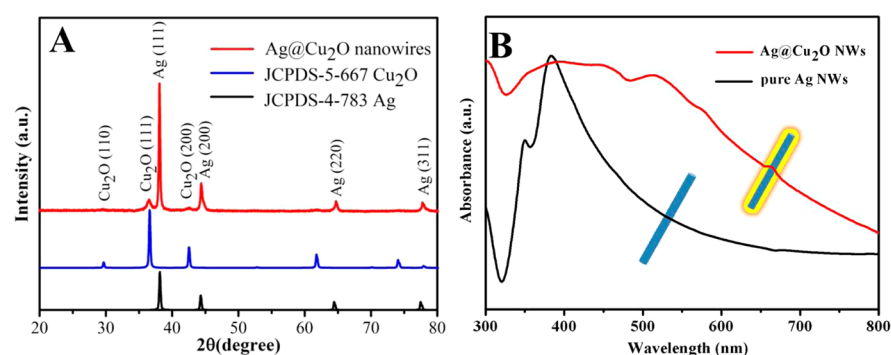

Figure 2. (A) XRD patterns and (B) UV−vis absorption spectra of as-prepared 1D Ag@Cu$_2$O core−shell heteronanowires and pure Ag NWs in ethanol.

nanowires is in agreement with the proposed Ag@Cu$_2$O composition. The spatial distribution of the colors verifies the core−shell structure, with an Ag core inside and Cu$_2$O shell outside. The composition of the core−shell heteronanowires was further confirmed by the energy-dispersive X-ray (EDX) spectrum (see Figure S3 in the Supporting Information). The EDX results also demonstrate that the as-prepared product is mainly composed of Ag, Cu, and O.

The crystalline structure and optical properties of the as-prepared Ag@Cu$_2$O core−shell heteronanowires are shown in Figure 2. The X-ray diffraction (XRD) pattern is compared with standard patterns of Ag (JCPDS 4−783) and Cu$_2$O (JCPDS 5−667) in Figure 2A, where every peak can be indexed to Ag or Cu$_2$O, supporting the formation of Ag@Cu$_2$O core−shell heteronanowires. The absence of other impurity peaks indicates the high purity of the core−shell Ag@Cu$_2$O heteronanowires fabricated by this simple solution process. In addition, the peaks of Cu$_2$O are characteristic of a cubic structure with a lattice constant of a = 4.27 Å. Its relatively weak peaks indicate the low crystallinity of Cu$_2$O shell relative to that of the Ag core. The X-ray photoelectron spectroscopy (XPS) results further confirm the successful synthesis of Ag@
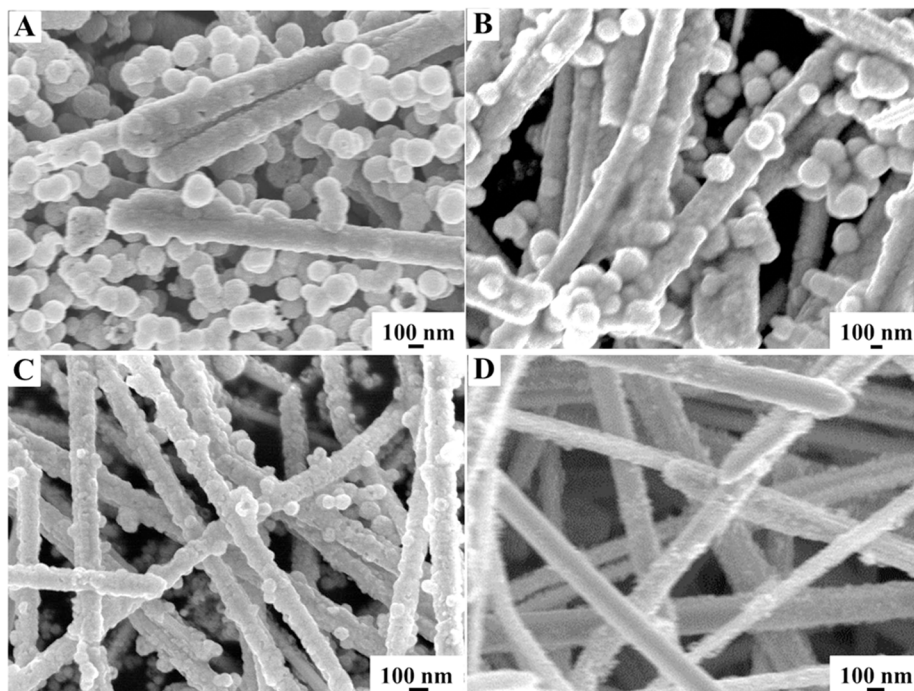
Figure 3. SEM images of the products prepared in the presence of different amounts of Ag solution: (A) 1, (B) 4, (C) 8, and (D) 16 mL.

Cu_2O core−shell heteronanowires (see Figure S4 in the Supporting Information).

Ag NWs show intense surface plasmon resonance (SPR) absorption in the visible region, which is highly sensitive to their diameter, length-to-diameter ratio, as well as the optical and electronic properties of their surroundings.[26,38,44−46] The ultraviolet−visible (UV−vis) absorption spectra of Ag@Cu_2O core−shell heteronanowires and pure Ag NWs in ethanol are presented in Figure 2B. The pure Ag NWs exhibit two absorbance peaks at 350 and 385 nm. The peak at 350 nm could be attributed to the longitudinal mode of nanowires similar to that of bulk Ag[38,47,48] or the out-of-plane quadrupole resonance of Ag NWs.[49−51] The peak at 385 nm is assigned to the transverse plasmon resonance of Ag NWs.[38,47,48] Upon the formation of Cu_2O shell, the transverse plasmon resonance of the Ag core is significantly red-shifted from 385 to 515 nm, due to the higher refractive index of Cu_2O (∼2.7 at wavelengths above 600 nm)[43,52,53] than ethanol (∼1.359)[27,38] and its high dielectric constant (e = 7.2).[43,52,54] Their broad absorbance from visible to UV window is crucial for full use of sunlight.

All the above results confirm our success in obtaining Ag@Cu_2O core−shell heteronanowires through this simple solution approach. Figures S5 and S6 in the Supporting Information present SEM images and UV−vis absorption of the core−shell heteronanowires collected at different reaction times. As shown in Figure 1A−C, before the growth of Cu_2O, the Ag NWs possess very smooth surfaces. After the Ag NWs were dispersed in $Cu(NO_3)_2$ solution, the heterogrowth of Cu_2O on the surface of the Ag NWs occurred immediately upon the addition of the reducing agent N_2H_4, accompanied by the rapid change of the reaction solution from gray to yellow. As shown in Figure S5A in the Supporting Information, a well-defined core−shell heterostructure with a rough surface was formed within 2 min, indicating that the formation of Cu_2O is very fast. As the growth reaction progresses, the obtained core−shell hetero-nanowires show no significant changes, and the surfaces of the

Ag NWs are totally covered by the Cu_2O nanoparticles (see Figure S5B−D in the Supporting Information). If the reaction was carried out for 12 h, however, some Cu_2O nanoparticles disappeared, and the smooth surface of the Ag NWs was observed (see Figure S5E in the Supporting Information). Further prolonging the reaction time to 24 h led to disappearance of most Cu_2O nanoparticles (see Figure S5F in the Supporting Information). These results indicate the reversibility of the Cu_2O reactions in our system. The reason for the gradual disappearance of the Cu_2O nanoparticles could be due to the gradual oxidation/dissolving of the Cu_2O by $NO_3^−$ ions in the acidic environment (see Figure S7 in the Supporting Information. The pH of reaction mixture is maintained between 3.72 and 3.03 within the initial 60 min; however, it is increased to 4.32 after reaction for 24 h. Therefore, the pH of the solution significantly influences the formation of the Cu_2O nanoparticles on the surface of the Ag NWs.

As shown in Figure S6 in the Supporting Information, the Ag@Cu_2O NWs obtained at 2, 20, 40, and 60 min exhibit similar absorption profiles, in which the SPR peak of Ag cores remained at 515 nm, and did not shift with the increase of reaction time. This means that Ag NWs were completely covered by sufficient Cu_2O shell (see Figure S5A−D in the Supporting Information), and their optical properties were not influenced by external surroundings.[52] The SPR peak of Ag cores in the product obtained at 12 h, however, shifted to shorter wavelength at 395 nm, principally due to the change in the refractive index of surroundings caused by the dearease in Cu_2O thickness. As shown in Figure S5E in the Supporting Information, Ag cores are not completely covered and some parts are exposed to solvent, which leads to the change in the effective refractive index of surroundings. The decrease in the refractive index causes the shift of SPR band to shorter wavelength.[52] The SPR peak in the product collected at 24 h shifted to 386 nm due to the disappearance of most Cu_2O
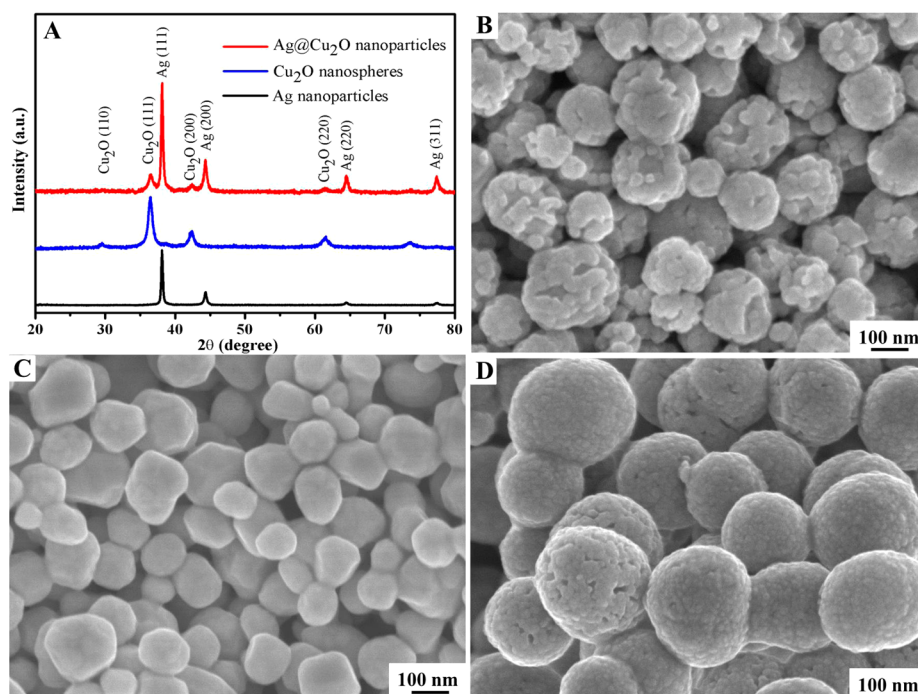
15719

dx.doi.org/10.1021/am502516s | ACS Appl. Mater. Interfaces 2014, 6, 15716−15725

Figure 4. (A) XRD patterns, and SEM images of (B) as-prepared Ag@Cu$_2$O nanoparticles, (C) Ag nanoparticles, and (D) pure Cu$_2$O.

shells (see Figure S5F in the Supporting Information), resulting in a similar spectrum to that of pure Ag NWs.

It should be noted that the amount of Ag NWs and Cu(NO$_3$)$_2$ solution also play important roles in the formation of Ag@Cu$_2$O core−shell heteronanowires. As shown in Figure 3(A), when 1 mL of Ag NW solution (∼0.038 mmol) is used, the Ag NWs are coated with many nanoparticles, while many free Cu$_2$O nanospheres with a diameter of about 200 nm are formed at the same time. The reason could be the fast formation of Cu$_2$O via the reduction of Cu(NO$_3$)$_2$ and insufficient amount of Ag NWs as anchoring sites, leading to the self-aggregation of the excessive produced Cu$_2$O nanocrystallites. Increasing the Ag NW solution to 4 mL (∼0.15 mmol) leads to an increase in the formation of Ag@Cu$_2$O core−shell NWs and a decrease in the fraction of free Cu$_2$O nanospheres [Figure 3(B)]. Further increasing the volume of the Ag NW solution to 8 mL (∼0.3 mmol) resulted in perfect Ag@Cu$_2$O core−shell heteronanowires. The Ag NWs are fully covered by Cu$_2$O nanoparticles, and there are almost no free-standing Cu$_2$O nanospheres to be found [Figure 3(C)]. A thin layer of very small nanoparticles are partly coated on the surfaces of Ag NWs, however, when the amount of Ag NW solution is further increased to 16 mL (∼0.6 mmol) (Figure 3D). Changing the amount/concentration of Cu(NO$_3$)$_2$ could not result in well-coated Ag@Cu$_2$O nanowires (see Figure S8 in the Supporting Information) either. The above results demonstrate that well-defined Ag@Cu$_2$O core−shell hetero-nanowires can only achieved be under certain conditions.

To demonstrate the applicability of our simple method, we prepared core−shell Ag@Cu$_2$O nanoparticles (NPs) under similar conditions by using Ag NPs as seeds. Pure Cu$_2$O NPs were also prepared in the absence of Ag for comparison. The resultant Ag@Cu$_2$O NPs and Cu$_2$O NPs were examined by XRD and SEM, respectively. The XRD results (Figure 4A and Figures S9−S11A in the Supporting Information) clearly reveal that all the diffraction peaks can be indexed to Ag (JCPDS 4−

783) and Cu$_2$O (JCPDS 5−667), and no other impurity diffraction peaks were observed. The SEM images (Figure 4B and Figure S9B−D in the Supporting Information) show that large quantities of Ag@Cu$_2$O NPs in the range of 100 to 230 nm have been successfully fabricated. The pure Cu$_2$O nanospheres have an average diameter of 440 nm (Figure 4D and Figure S10B−D in the Supporting Information). These results demonstrate that the final morphology of the Ag@Cu$_2$O nanostructures greatly depends on the morphology of the Ag seeds.

The resultant Ag@Cu$_2$O core−shell nanowires and nanoparticles are expected to show higher photocatalytic activity than pure Cu$_2$O NPs, because of the plasmonic enhancment of the Ag cores. The performance of the Ag@Cu$_2$O NWs, Ag@Cu$_2$O NPs, and pure Cu$_2$O nanospheres was evaluated by the photodegradation of MO under solar light irradiation. For comparison, the Ag NWs were also tested under identical experimental conditions. Figure 5A−C shows the absorption spectra of MO solutions after photocatalytic degradation for various durations over Ag@Cu$_2$O NWs, Ag@Cu$_2$O NPs, and pure Cu$_2$O nanospheres, respectively. Under solar light irradiation, the absorption peak at 464 nm diminishes gradually as the irradiation time increases. As shown in Figure 5D, it can be clearly observed that in the absence of catalyst and in the presence of only Ag NWs under solar light irradiation, there is no evident photodegradation of MO. In contrast, the as-prepared Ag@Cu$_2$O NWs, Ag@Cu$_2$O NPs, and pure Cu$_2$O nanospheres all exhibit excellent photocatalytic performance. Moreover, both the core−shell Ag@Cu$_2$O NWs and the Ag@Cu$_2$O NPs show higher photocatalytic activity than that of the pure Cu$_2$O nanospheres, while the Ag@Cu$_2$O core−shell NWs exhibit the highest performance, which can decolor 92% of MO within 140 min, whereas 83 and 71% of MO can be degraded over the Ag@Cu$_2$O NPs and pure Cu$_2$O nanospheres, respectively. In compared with previously reported Ag@Cu$_2$O nanoparticles and Cu$_2$O−Au composites, our nanostructures
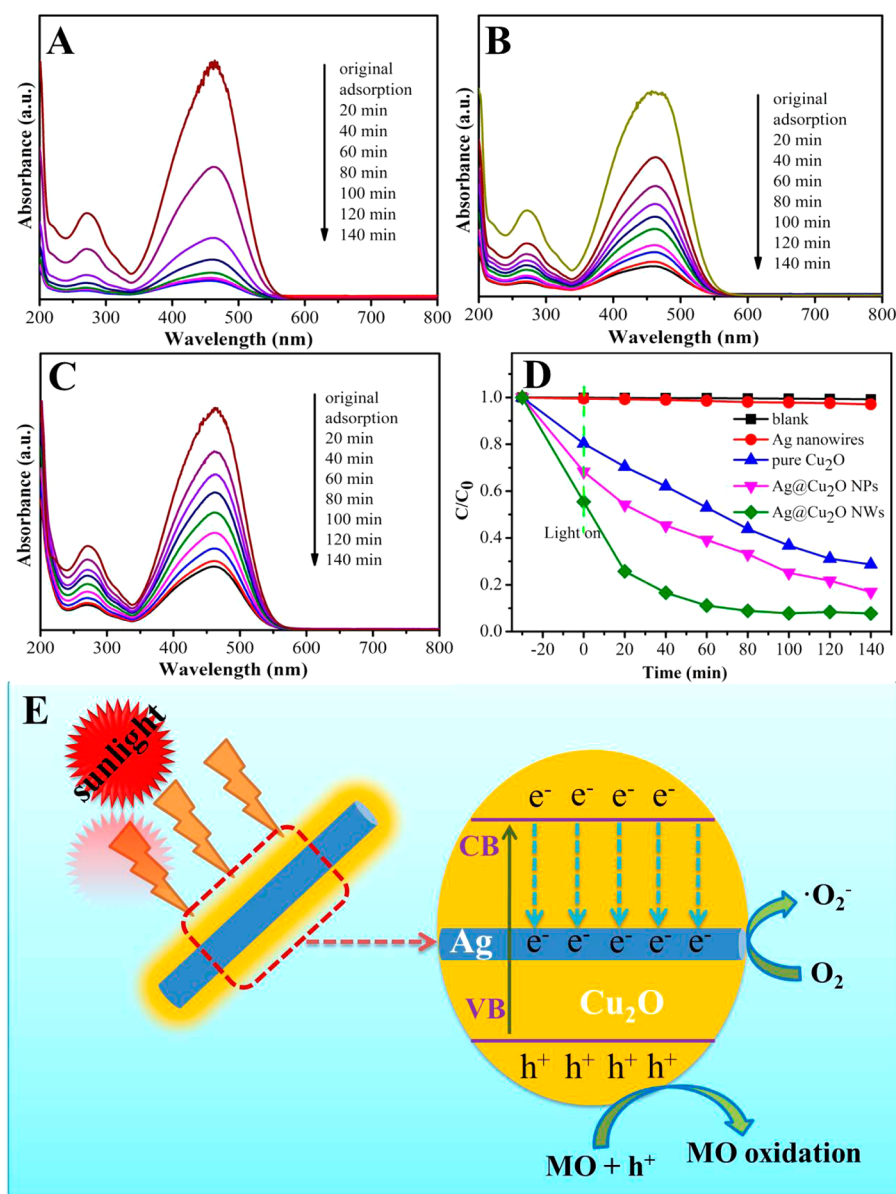
Figure 5. (A−C) Variation in the light absorption of the MO solution in the presence of the as-prepared photocatalysts under solar light irradiation for different irradiation times: (A) Ag@Cu$_2$O NWs, (B) Ag@Cu$_2$O NPs, and (C) pure Cu$_2$O nanospheres. (D) Photocatalytic activity of MO oxidation under solar light irradiation. (E) Schematic illustration of the transfer of photogenerated electron−hole pairs in the Ag@Cu$_2$O core−shell NWs under solar light irradiation.

exhibit higher photoactivity in degradation of MO, e.g. 90% MO can be degraded by core−shell Ag@Cu$_2$O NWs within 2 h, but only ∼75% MO was degraded by the Ag@Cu$_2$O nanoparticles within the same time[26] and ∼60% MO was degraded within 4 h by Cu$_2$O−Au composites.[55] The results clearly demonstrate that the heterogrowth of Cu$_2$O nanoshells on Ag NWs to build 1D core−shell heterostructures has been proven to be a useful and successful strategy for improving the photocatalytic properties of Cu$_2$O crystals.

To better understand the good performance of our core−shell Ag@Cu$_2$O NWs, their XRD, XPS, SEM, and TEM characterizations have been conducted after photocatalytic test. The XRD pattern shows that the dominant peaks of Cu$_2$O (111) and (200) become much weaker after photocatalysis test (see Figure S12A in the Supporting Information). In addition, there is no other peaks detected except that of Ag nanowires. The binding energies measured by XPS show two peaks at

934.4 and 954.2 eV, which are respectively assigned to Cu 2p3/2 and Cu 2p1/2 of copper ions. Devolution of Cu 2p peaks into Cu^{2+} and Cu$^+$ revealed two small peaks of Cu$^+$ from Cu$_2$O at 932.6 and 952.3 eV, respectively (see Figure S12B in the Supporting Information). The peaks of Cu^{2+} stronger than that of Cu$^+$ after photocatalytic test suggest a dense protection layer of CuO or Cu(OH)$_2$ on the surface of Cu$_2$O.

It should be noted that the morphology of photocatalysts changed after photocatalytic test. There are many sheetlike structures and uncovered Ag NWs formed due to the loss of Cu$_2$O nanoparticles (see Figure S12C in the Supporting Information). The TEM image in Figure S12D in the Supporting Information further confirms the loss of Cu$_2$O nanoparticles and the decrease in their density on the surface of Ag NWs. This result is similar to the previous reports,[29,56] and the morphology transformation could be explained as follows. Cu$_2$O nanoparticles are irradiated by solar light to produce

electrons and holes. On the one hand, the photogenerated electrons quickly transferred and accumulated in Ag NWs, which further transferred to O_2 molecules adsorbed on the surface, and facilitated their multiple-electron reduction reactions. The formed reactive species ($\bullet O_2^-$) can effectively bleach the dye. On the other hand, Cu_2O are oxidized into CuO by the accumulated holes in them, and the intermediate CuO can also generate electron−hole pairs under irradiation of solar light. As the photogenerated holes are captured by MO and the accumulated electrons can reduce CuO into Cu_2O, accompanied by the formation of sheet structure.

It was reported that in the photodegradation of organic pollutants, reactive species such as $\bullet O_2^-$, h^+, and $\bullet OH$ played as bridge role of photocatalysts under the light irradiation,[57−60] and they could vary with the different photocatalysts.[61,62] To investigate the photocatalytic mechanism and to understand the better performance of 1D Ag@Cu_2O core−shell phtocatalysts, the effect of scavengers on the degradation of MO was examined to clarify the contribution of different reactive species during photocatalysis study. We used p-benzoquinone (PBQ) as $\bullet O_2^-$ scavengers,[57−60,63−65] triethanolamine (TEOA) as h^+ scavengers,[61,62,65] and isopropanol (IPA) as $\bullet OH$ scavengers.[63,66] These scavengers were added into the MO solution together with the 1D Ag@Cu_2O core−shell heteronanowires before irradiation. As depicted in Figure 6, the complete
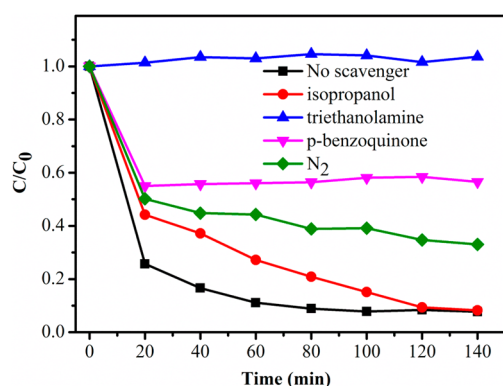

Figure 6. Photocatalytic degradation of MO over the 1D Ag@Cu_2O core−shell heteronanowires in the presence of scavengers.

inhibition of degradation of MO in the presence of TEOA suggests that photogenerated holes are the major reactive species for the photocatalytic degradation of MO. The dramatic decrease in degradation of MO arising from removal of oxygen with N_2 bubbling demonstrates that molecular oxygen also played an important role in the photodegradation of MO over 1D Ag@Cu_2O core−shell heteronanowires. This is attributed to the electron trapping role of molecular oxygen, which could produce $\bullet O_2^-$ to inhibit the recombination of electron−hole pairs and leave over holes to oxidize MO. The elimination of molecular oxygen would diminish the amount of holes and prevent the oxidation of MO due to the fast combination of electron−hole pairs. In order to confirm the roles of $\bullet O_2^-$ in the degradation of MO, we employed PBQ as the $\bullet O_2^-$ scavenger. The results show that the presence of PBQ significantly decreased the MO photodegradation efficiency from 92% to 45% within 140 min for 1D Ag@Cu_2O core−shell heteronanowires. In contrast, the addition of IPA had little effect on the MO degradation. The above results illustrate that both h^+ and $\cdot O_2^-$ are the main reactive species for 1D Ag@

Cu_2O core−shell heteronanowires in the photocatalytic decolorization of MO under solar light irradiation, and the reactive $\cdot OH$ preferred to react with MO dye, because of the presence of N═N double bond and benzene ring in the azo-dye MO molecules, which are more reactive than the hydroxyl group in IPA.

The drastic enhancement in photocatalytic activity of the 1D core−shell Ag@Cu_2O NWs may be ascribed to the synergistic effects of Ag NWs and surface Cu_2O. As evidenced by SEM and TEM images, there are clear interfaces between Ag NWs and Cu_2O nanoparticles, which can effectively suppress the recombination rate of electron−hole pairs.[67] More specifically, first, the direct coupling of Ag NWs and Cu_2O causes the Fermi level to equilibrate, which can lead to trapping of charges and increase carrier life.[26] The Ag NWs in the core−shell structures produce a Schottky barrier at the interface between the core and shell, which facilitates the capture and quick transfer of photoexcited electrons from the Cu_2O nanoshells to the Ag NWs under solar light irradiation (Figure 5E).[25,67,68] The electrons accumulated in the Ag NWs are transferred to O_2 molecules to produce superoxide radical anions ($\bullet O_2^-$) through the multiple-electron reduction reactions to decompose organic pollutant.[39] Accumulation of the photoinduced holes in the valence band of the Cu_2O nanoshells leads to the production of the hydroxyl radical ($\bullet OH$) at the surface, which is responsible for the oxidation decomposition of the MO molecules.[25] Photoexcited electrons are effectively accumulated in the Ag NWs without recombining with holes, which could promote the effective separation of photogenerated electron−hole pairs. This leads to the significant enhancement of the photocatalytic activity of the Ag@Cu_2O core−shell structures. Second, the unique 1D Ag@Cu_2O core−shell nanostructures are expected to have excellent electron conductivity and mobility. The presence of metal nanowires can facilitate fast and long-distance electron transport, and the fast transfer of photoinduced electrons and holes over the Ag NWs and Cu_2O nanoshells suppresses the recombination of electron−hole pairs, which is favorable for highly efficient photocatalytic performance. Third, the core−shell Ag@Cu_2O nanowires have a large specific surface area for adsorbing dyes (45, 32, and 20% MO adsorption in the dark equilibration for Ag@Cu_2O NWs (10.3 m^2/g), Ag@Cu_2O NPs (8.8 m^2/g), and pure Cu_2O nanospheres, respectively, in our experiment), which can provide more active sites for the photodegradation of MO and thus promote diffusion of reactants and products during the reaction, accelerating the chemical reactions. Fourth, the high length-to-diameter ratio of the 1D metal-core@semi-conductor-shell heteronanostructures may remarkablely enhance the light absorption, trapping, and scattering through a local field enhancement effect of plasmonic Ag NWs,[69] and thus increase the quantity of photogenerated electrons and holes available to participate in the photocatalytic reactions, leading to an enhanced photocatalytic property of the Cu_2O.[68] It should be noted, however, that the photocatalytic mechanism over such 1D Ag@Cu_2O core−shell heteronanowires is still not completely understood, and a more detailed study is still underway.

4. CONCLUSION

In summary, 1D core−shell Ag@Cu_2O heteronanowires have been fabricated by a facile solution process at room temperature. The resulting unique heterostructures exhibit greater plasmonic enhancement of photocatalytic activity in

MO oxidizing than Ag@Cu_2O nanoparticles and pure Cu_2O under solar light irradiation. Such rational design and fabrication of 1D metal-core@semiconductor-shell architectures may hold great potential in solar energy conversion, especially as an effective technique to improve photocatalytic activity.

■ ASSOCIATED CONTENT

ⓢ Supporting Information

Additional characterization data including XRD pattern of Ag NWs, HRTEM images, EDS pattern and XPS spectra of 1D Ag@Cu_2O core−shell heteronanowires, SEM images and UV−vis absorption spectra of the products obtained at different reaction times, SEM images of the products prepared from different concentration of $Cu(NO_3)_2$, the photographs of reaction systems composited of Ag NWs, $Cu(NO_3)_2$ solution and N_2H_4 before and after reaction at different stages, and XRD patterns and SEM images of Ag@Cu_2O NPs, Ag NPs, and pure Cu_2O, XRD pattern, XPS spectrum of Cu 2p, SEM image and TEM image of 1D Ag@Cu_2O core−shell heteronanowires after photocatalytic test. This material is available free of charge via the Internet at http://pubs.acs.org.

■ AUTHOR INFORMATION

Corresponding Author
*E-mail: zhenl@uow.edu.au. Tel: +61-2-42215163. Fax +61-2-42215731.

Notes
The authors declare no competing financial interest.

■ ACKNOWLEDGMENTS

■ REFERENCES

(1) Shankar, K.; Basham, J. I.; Allam, N. K.; Varghese, O. K.; Mor, G. K.; Feng, X.; Paulose, M.; Seabold, J. A.; Choi, K.-S.; Grimes, C. A. Recent Advances in the Use of TiO_2 Nanotube and Nanowire Arrays for Oxidative Photoelectrochemistry. *J. Phys. Chem. C* 2009, 113, 6327−6359.

(2) Martinson, A. B. F.; McGarrah, J. E.; Parpia, M. O. K.; Hupp, J. T. Dynamics of Charge Transport and Recombination in ZnO Nanorod Array Dye-Sensitized Solar Cells. *Phys. Chem. Chem. Phys.* 2006, 8, 4655−4659.

(3) Ohsaki, Y.; Masaki, N.; Kitamura, T.; Wada, Y.; Okamoto, T.; Sekino, T.; Niihara, K.; Yanagida, S. Dye-Sensitized TiO_2 Nanotube Solar Cells: Fabrication and Electronic Characterization. *Phys. Chem. Chem. Phys.* 2005, 7, 4157−4163.

(4) Tachikawa, T.; Tojo, S.; Fujitsuka, M.; Sekino, T.; Majima, T. Photoinduced Charge Separation in Titania Nanotubes. *J. Phys. Chem. B* 2006, 110, 14055−14059.

(5) Tang, Z.-R.; Li, F.; Zhang, Y.; Fu, X.; Xu, Y.-J. Composites of Titanate Nanotube and Carbon Nanotube as Photocatalyst with High Mineralization Ratio for Gas-Phase Degradation of Volatile Aromatic Pollutant. *J. Phys. Chem. C* 2011, 115, 7880−7886.

(6) Wu, N.; Wang, J.; Tafen, D. N.; Wang, H.; Zheng, J.-G.; Lewis, J. P.; Liu, X.; Leonard, S. S.; Manivannan, A. Shape-Enhanced Photocatalytic Activity of Single-Crystalline Anatase TiO_2 (101) Nanobelts. *J. Am. Chem. Soc.* 2010, 132, 6679−6685.

(7) Liu, Z.; Zhang, X.; Nishimoto, S.; Murakami, T.; Fujishima, A. Efficient Photocatalytic Degradation of Gaseous Acetaldehyde by Highly Ordered TiO_2 Nanotube Arrays. *Environ. Sci. Technol.* 2008, 42, 8547−8551.

(8) Weng, B.; Liu, S.; Tang, Z.-R.; Xu, Y.-J. One-Dimensional Nanostructure-Based Materials for Versatile Photocatalytic Applications. *RSC Adv.* 2014, 4, 12685−12700.

(9) Jennings, J. R.; Ghicov, A.; Peter, L. M.; Schmuki, P.; Walker, A. B. Dye-Sensitized Solar Cells Based on Oriented TiO_2 Nanotube Arrays: Transport, Trapping, and Transfer of Electrons. *J. Am. Chem. Soc.* 2008, 130, 13364−13372.

(10) Tachikawa, T.; Majima, T. Exploring the Spatial Distribution and Transport Behavior of Charge Carriers in a Single Titania Nanowire. *J. Am. Chem. Soc.* 2009, 131, 8485−8495.

(11) Tang, Z.-R.; Yin, X.; Zhang, Y.; Xu, Y.-J. One-Pot, High-Yield Synthesis of One-Dimensional ZnO Nanorods with Well-Defined Morphology as a Highly Selective Photocatalyst. *RSC Adv.* 2013, 3, 5956−5965.

(12) Bai, X.; Wang, L.; Zong, R.; Zhu, Y. Photocatalytic Activity Enhanced via g-C_3N_4 Nanoplates to Nanorods. *J. Phys. Chem. C* 2013, 117, 9952−9961.

(13) Li, Z.; Cheng, L.; Sun, Q.; Zhu, Z.; Riley, M. J.; Aljada, M.; Cheng, Z.; Wang, X.; Hanson, G. R.; Qiao, S.; Smith, S. C.; Lu, G. Q. Diluted Magnetic Semiconductor Nanowires Prepared by the Solution-Liquid-Solid Method. *Angew. Chem., Int. Ed.* 2010, 49, 2777−2781.

(14) Li, Z.; Kurtulus, Ö.; Fu, N.; Wang, Z.; Kornowski, A.; Pietsch, U.; Mews, A. Controlled Synthesis of CdSe Nanowires by Solution-Liquid-Solid Method. *Adv. Funct. Mater.* 2009, 19, 3650−3661.

(15) Li, Z.; Du, A. J.; Sun, Q.; Aljada, M.; Cheng, L. N.; Riley, M. J.; Zhu, Z. H.; Cheng, Z. X.; Wang, X. L.; Hall, J.; Krausz, E.; Qiao, S. Z.; Smith, S. C.; Lu, G. Q. Cobalt-Doped Cadmium Selenide Colloidal Nanowires. *Chem. Commun.* 2011, 47, 11894−11896.

(16) Li, Z.; Ma, X.; Sun, Q.; Wang, Z.; Liu, J.; Zhu, Z.; Qiao, S. Z.; Smith, S. C.; Lu, G.; Mews, A. Synthesis and Characterization of Colloidal Core-Shell Semiconductor Nanowires. *Eur. J. Inorg. Chem.* 2010, 2010, 4325−4331.

(17) Kudo, A.; Miseki, Y. Heterogeneous Photocatalyst Materials for Water Splitting. *Chem. Soc. Rev.* 2009, 38, 253−278.

(18) Tian, C.; Zhang, Q.; Wu, A.; Jiang, M.; Liang, Z.; Jiang, B.; Fu, H. Cost-Effective Large-Scale Synthesis of ZnO Photocatalyst with Excellent Performance for Dye Photodegradation. *Chem. Commun.* 2012, 48, 2858−2860.

(19) Liu, G.; Wang, L.; Yang, H. G.; Cheng, H.-M.; Lu, G. Q. Titania-Based Photocatalysts-Crystal Growth, Doping and Heterostructuring. *J. Mater. Chem.* 2010, 20, 831−843.

(20) Wang, J.; Tafen, D. N.; Lewis, J. P.; Hong, Z.; Manivannan, A.; Zhi, M.; Li, M.; Wu, N. Origin of Photocatalytic Activity of Nitrogen-Doped TiO_2 Nanobelts. *J. Am. Chem. Soc.* 2009, 131, 12290−12297.

(21) Hou, W.; Cronin, S. B. A Review of Surface Plasmon Resonance-Enhanced Photocatalysis. *Adv. Funct. Mater.* 2013, 23, 1612−1619.

(22) Wang, P.; Huang, B.; Dai, Y.; Whangbo, M.-H. Plasmonic Photocatalysts: Harvesting Visible Light with Noble Metal Nanoparticles. *Phys. Chem. Chem. Phys.* 2012, 14, 9813−9825.

(23) Cushing, S. K.; Li, J.; Meng, F.; Senty, T. R.; Suri, S.; Zhi, M.; Li, M.; Bristow, A. D.; Wu, N. Photocatalytic Activity Enhanced by Plasmonic Resonant Energy Transfer from Metal to Semiconductor. *J. Am. Chem. Soc.* 2012, 134, 15033−15041.

(24) Xiao, F. Layer-by-Layer Self-Assembly Construction of Highly Ordered Metal-TiO_2 Nanotube Arrays Heterostructures (M/TNTs, M = Au, Ag, Pt) with Tunable Catalytic Activities. *J. Phys. Chem. C* 2012, 116, 16487−16498.

(25) Cheng, B.; Le, Y.; Yu, J. Preparation and Enhanced Photocatalytic Activity of Ag@TiO_2 Core-Shell Nanocomposite Nanowires. *J. Hazard. Mater.* 2010, 177, 971−977.

(26) Li, J.; Cushing, S. K.; Bright, J.; Meng, F.; Senty, T. R.; Zheng, P.; Bristow, A. D.; Wu, N. Ag@Cu$_2$O Core-Shell Nanoparticles as Visible-Light Plasmonic Photocatalysts. *ACS Catal.* **2013**, *3*, 47–51.

(27) Hirakawa, T.; Kamat, P. V. Charge Separation and Catalytic Activity of Ag@TiO$_2$ Core-Shell Composite Clusters under UV-Irradiation. *J. Am. Chem. Soc.* **2005**, *127*, 3928–3934.

(28) Zhao, Y.; Wang, W.; Li, Y.; Zhang, Y.; Yan, Z.; Huo, Z. Hierarchical Branched Cu$_2$O Nanowires with Enhanced Photocatalytic Activity and Stability for H$_2$ Production. *Nanoscale* **2014**, *6*, 195–198.

(29) Zheng, Z.; Huang, B.; Wang, Z.; Guo, M.; Qin, X.; Zhang, X.; Wang, P.; Dai, Y. Crystal Faces of Cu$_2$O and Their Stabilities in Photocatalytic Reactions. *J. Phys. Chem. C* **2009**, *113*, 14448–14453.

(30) Zhang, Y.; Deng, B.; Zhang, T.; Gao, D.; Xu, A.-W. Shape Effects of Cu$_2$O Polyhedral Microcrystals on Photocatalytic Activity. *J. Phys. Chem. C* **2010**, *114*, 5073–5079.

(31) Wang, M.; Sun, L.; Lin, Z.; Cai, J.; Xie, K.; Lin, C. p-n Heterojunction Photoelectrodes Composed of Cu$_2$O-Loaded TiO$_2$ Nanotube Arrays with Enhanced Photoelectrochemical and Photo-electrocatalytic Activities. *Energy Environ. Sci.* **2013**, *6*, 1211–1220.

(32) Cheng, W.-Y.; Yu, T.-H.; Chao, K.-J.; Lu, S.-Y. Cu2O-Decorated Mesoporous TiO$_2$ Beads as a Highly Efficient Photocatalyst for Hydrogen Production. *ChemCatChem.* **2014**, *6*, 293–300.

(33) Wang, Y.; Yu, K.; Yin, H.; Song, C.; Zhang, Z.; Li, S.; Shi, H.; Zhang, Q.; Zhao, B.; Zhang, Y.; Zhu, Z. Facile Synthesis, Enhanced Field Emission and Photocatalytic Activities of Cu$_2$O-TiO$_2$-ZnO Ternary Hetero-Nanostructures. *J. Phys. D: Appl. Phys.* **2013**, *46*, 175303.

(34) Ai, Z.; Zhang, L.; Lee, S.; Ho, W. Interfacial Hydrothermal Synthesis of Cu@Cu$_2$O Core-Shell Microspheres with Enhanced Visible-Light-Driven Photocatalytic Activity. *J. Phys. Chem. C* **2009**, *113*, 20896–20902.

(35) Kuo, C.-H.; Yang, Y.-C.; Gwo, S.; Huang, M. H. Facet-Dependent and Au Nanocrystal-Enhanced Electrical and Photo-catalytic Properties of Au-Cu$_2$O Core-Shell Heterostructures. *J. Am. Chem. Soc.* **2010**, *133*, 1052–1057.

(36) Fan, W.; Jewell, S.; She, Y.; Leung, M. K. H. In Situ Deposition of Ag-Ag$_2$S Hybrid Nanoparticles onto TiO$_2$ Nanotube Arrays towards Fabrication of Photoelectrodes with High Visible Light Photo-electrochemical Properties. *Phys. Chem. Chem. Phys.* **2014**, *16*, 676–680.

(37) Su, C.; Liu, L.; Zhang, M.; Zhang, Y.; Shao, C. Fabrication of Ag/TiO$_2$ Nanoheterostructures with Visible Light Photocatalytic Function via a Solvothermal Approach. *CrystEngComm* **2012**, *14*, 3989–3999.

(38) Ramasamy, P.; Seo, D.-M.; Kim, S.-H.; Kim, J. Effects of TiO$_2$ Shells on Optical and Thermal Properties of Silver Nanowires. *J. Mater. Chem.* **2012**, *22*, 11651–11657.

(39) Hu, H.; Jiao, Z.; Wang, T.; Ye, J.; Lu, G.; Bi, Y. Enhanced Photocatalytic Activity of Ag/Ag$_3$PO$_4$ Coaxial Hetero-Nanowires. *J. Mater. Chem. A* **2013**, *1*, 10612–10616.

(40) Bi, Y.; Hu, H.; Ouyang, S.; Jiao, Z.; Lu, G.; Ye, J. Selective Growth of Ag$_3$PO$_4$ Submicro-Cubes on Ag Nanowires to Fabricate Necklace-Like Heterostructures for Photocatalytic Applications. *J. Mater. Chem.* **2012**, *22*, 14847–14850.

(41) Bi, Y.; Ye, J. In Situ Oxidation Synthesis of Ag/AgCl Core-Shell Nanowires and Their Photocatalytic Properties. *Chem. Commun.* **2009**, 6551–6553.

(42) Wiley, B.; Sun, Y.; Xia, Y. Synthesis of Silver Nanostructures with Controlled Shapes and Properties. *Acc. Chem. Res.* **2007**, *40*, 1067–1076.

(43) Zhang, L.; Blom, D. A.; Wang, H. Au-Cu$_2$O Core–Shell Nanoparticles: A Hybrid Metal-Semiconductor Heteronanostructure with Geometrically Tunable Optical Properties. *Chem. Mater.* **2011**, *23*, 4587–4598.

(44) Callegari, A.; Tonti, D.; Chergui, M. Photochemically Grown Silver Nanoparticles with Wavelength-Controlled Size and Shape. *Nano Lett.* **2003**, *3*, 1565–1568.

(45) Jin, R.; Cao, Y.; Mirkin, C. A.; Kelly, K. L.; Schatz, G. C.; Zheng, J. G. Photoinduced Conversion of Silver Nanospheres to Nanoprisms. *Science* **2001**, *294*, 1901–1903.

(46) Mulvaney, P. Surface Plasmon Spectroscopy of Nanosized Metal Particles. *Langmuir* **1996**, *12*, 788–800.

(47) Wang, Z.; Liu, J.; Chen, X.; Wan, J.; Qian, Y. A Simple Hydrothermal Route to Large-Scale Synthesis of Uniform Silver Nanowires. *Chem.—Eur. J.* **2005**, *11*, 160–163.

(48) Sun, Y.; Gates, B.; Mayers, B.; Xia, Y. Crystalline Silver Nanowires by Soft Solution Processing. *Nano Lett.* **2002**, *2*, 165–168.

(49) Chen, S.; Carroll, D. L. Synthesis and Characterization of Truncated Triangular Silver Nanoplates. *Nano Lett.* **2002**, *2*, 1003–1007.

(50) Jin, R.; Charles Cao, Y.; Hao, E.; Metraux, G. S.; Schatz, G. C.; Mirkin, C. A. Controlling Anisotropic Nanoparticle Growth through Plasmon Excitation. *Nature* **2003**, *425*, 487–490.

(51) Gao, Y.; Song, L.; Jiang, P.; Liu, L. F.; Yan, X. Q.; Zhou, Z. P.; Liu, D. F.; Wang, J. X.; Yuan, H. J.; Zhang, Z. X.; Zhao, X. W.; Dou, X. Y.; Zhou, W. Y.; Wang, G.; Xie, S. S.; Chen, H. Y.; Li, J. Q. Silver Nanowires with Five-Fold Symmetric Cross-Section. *J. Cryst. Growth* **2005**, *276*, 606–612.

(52) Yang, Y.-C.; Wang, H.-J.; Whang, J.; Huang, J.-S.; Lyu, L.-M.; Lin, P.-H.; Gwo, S.; Huang, M. H. Facet-Dependent Optical Properties of Polyhedral Au-Cu$_2$O Core-Shell Nanocrystals. *Nanoscale* **2014**, *6*, 4316–4324.

(53) Rai, P.; Khan, R.; Raj, S.; Majhi, S. M.; Park, K.-K.; Yu, Y.-T.; Lee, I.-H.; Sekhar, P. K. Au@Cu$_2$O Core-Shell Nanoparticles as Chemiresistors for Gas Sensor Applications: Effect of Potential Barrier Modulation on the Sensing Performance. *Nanoscale* **2014**, *6*, 581–588.

(54) Bardhan, R.; Grady, N. K.; Ali, T.; Halas, N. J. Metallic Nanoshells with Semiconductor Cores: Optical Characteristics Modified by Core Medium Properties. *ACS Nano* **2010**, *4*, 6169–6179.

(55) Hua, Q.; Shi, F.; Chen, K.; Chang, S.; Ma, Y.; Jiang, Z.; Pan, G.; Huang, W. Cu$_2$O-Au Nanocomposites with Novel Structures and Remarkable Chemisorption Capacity and Photocatalytic Activity. *Nano Res.* **2011**, *4*, 948–962.

(56) Pan, L.; Zou, J.-J.; Zhang, T.; Wang, S.; Li, Z.; Wang, L.; Zhang, X. Cu$_2$O Film via Hydrothermal Redox Approach: Morphology and Photocatalytic Performance. *J. Phys. Chem. C* **2014**, *118*, 16335–16343.

(57) Cao, J.; Luo, B.; Lin, H.; Xu, B.; Chen, S. Visible Llight Photocatalytic Activity Enhancement and Mechanism of AgBr/Ag$_3$PO$_4$ Hybrids for Degradation of Methyl Orange. *J. Hazard. Mater.* **2012**, *217–218*, 107–115.

(58) Yin, M.; Li, Z.; Kou, J.; Zou, Z. Mechanism Investigation of Visible Light-Induced Degradation in a Heterogeneous TiO$_2$/Eosin Y/Rhodamine B System. *Environ. Sci. Technol.* **2009**, *43*, 8361–8366.

(59) Cao, J.; Li, X.; Lin, H.; Chen, S.; Fu, X. In Situ Preparation of Novel p-n Junction Photocatalyst BiOI/(BiO)$_2$CO$_3$ with Enhanced Visible Light Photocatalytic Activity. *J. Hazard. Mater.* **2012**, *239–240*, 316–324.

(60) Lin, H.; Ye, H.; Chen, S.; Chen, Y. One-Pot Hydrothermal Synthesis of BiPO$_4$/BiVO$_4$ with Enhanced Visible-light Photocatalytic Activities for Methylene Blue Degradation. *RSC Adv.* **2014**, *4*, 10968–10974.

(61) Chen, L.; Huang, R.; Yin, S.-F.; Luo, S.-L.; Au, C.-T. Flower-Like Bi$_2$O$_2$CO$_3$: Facile Synthesis and Their Photocatalytic Application in Treatment of Dye-Containing Wastewater. *Chem. Eng. J.* **2012**, *193–194*, 123–130.

(62) Yuan, Q.; Chen, L.; Xiong, M.; He, J.; Luo, S.-L.; Au, C.-T.; Yin, S.-F. Cu$_2$O/BiVO$_4$ Heterostructures: Synthesis and Application in Simultaneous Photocatalytic Oxidation of Organic Dyes and Reduction of Cr(VI) under Visible Light. *Chem. Eng. J.* **2014**, *255*, 394–402.

(63) Zhou, J.; Tian, G.; Chen, Y.; Shi, Y.; Tian, C.; Pan, K.; Fu, H. Growth Rate Controlled Synthesis of Hierarchical Bi$_2$S$_3$/In$_2$S$_3$ Core/Shell Microspheres with Enhanced Photocatalytic Activity. *Sci. Rep.* **2014**, *4*, 4027.

(64) Katsumata, H.; Sakai, T.; Suzuki, T.; Kaneco, S. Highly Efficient Photocatalytic Activity of g-C_3N_4/Ag_3PO_4 Hybrid Photocatalysts through Z-Scheme Photocatalytic Mechanism under Visible Light. *Ind. Eng. Chem. Res.* **2014**, *53*, 8018−8025.

(65) Ding, X.; Zhao, K.; Zhang, L. Enhanced Photocatalytic Removal of Sodium Pentachlorophenate with Self-Doped Bi_2WO_6 under Visible Light by Generating More Superoxide Ions. *Environ. Sci. Technol.* **2014**, *48*, 5823−5831.

(66) Chelnokov, E.; Cuba, V.; Simeone, D.; Guigner, J. M.; Schmidhammer, U.; Mostafavi, M.; Le Caër, S. Electron Transfer at Oxide/Water Interfaces Induced by Ionizing Radiation. *J. Phys. Chem. C* **2014**, *118*, 7865−7873.

(67) Wang, H.; Zhang, L.; Chen, Z.; Hu, J.; Li, S.; Wang, Z.; Liu, J.; Wang, X. Semiconductor Heterojunction Photocatalysts: Design, Construction, and Photocatalytic Performances. *Chem. Soc. Rev.* **2014**, *43*, 5234−5244.

(68) Pan, Y.; Deng, S.; Polavarapu, L.; Gao, N.; Yuan, P.; Sow, C. H.; Xu, Q.-H. Plasmon-Enhanced Photocatalytic Properties of Cu_2O Nanowire-Au Nanoparticle Assemblies. *Langmuir* **2012**, *28*, 12304−12310.

(69) Qu, Y.; Cheng, R.; Su, Q.; Duan, X. Plasmonic Enhancements of Photocatalytic Activity of Pt/n-Si/Ag Photodiodes Using Au/Ag Core/Shell Nanorods. *J. Am. Chem. Soc.* **2011**, *133*, 16730−16733.